Characterization of Two Distinct Modes of Drug Binding to Human Intestinal Fatty Acid Binding Protein

Rahul Patil[1], Aisha Laguerre[1], Jerome Wielens[1,2,3], Stephen J. Headey[1], Martin L. Williams[1], Maria L. R. Hughes[1], Biswaranjan Mohanty[1], Christopher J. H. Porter[4], Martin J. Scanlon[1]

[1]Medicinal Chemistry, and [4]Drug Delivery, Disposition and Dynamics, Monash Institute of Pharmaceutical Sciences, Monash University, 381 Royal Parade, Parkville, Victoria 3052 (Australia)

[2]ACRF Rational Drug Discovery Centre and Biota Structural Biology Laboratory, St Vincent's Institute of Medical Research, 9 Princes Street, Fitzroy, Victoria 3056 (Australia)

[3]Department of Medicine, University of Melbourne, 41 Victoria Parade, Fitzroy, Victoria 3065 (Australia)

ABSTRACT

The aqueous cytoplasm of cells poses a potentially significant barrier for many lipophilic drugs to reach their sites of action. Fatty acid binding proteins (FABPs) bind to poorly water–soluble fatty acids (FAs) and lipophilic compounds and facilitate their intracellular transport. Several structures of FA in complex with FABPs have been described, but data describing the binding sites of other lipophilic ligands including drugs are limited. Here the environmentally sensitive fluorophores, 1–anilinonapthalene 8–sulfonic acid (ANS), and 11–dansylamino undecanoic acid (DAUDA) were used to investigate drug binding to human intestinal FABP (hIFABP). Most drugs that bound hIFABP were able to displace both ANS and DAUDA. A notable exception was ketorolac, a non–steroidal anti–inflammatory drug that bound to hIFABP and displaced DAUDA but failed to displace ANS. Isothermal titration calorimetry revealed that for the majority of ligands including FA, ANS and DAUDA, binding to hIFABP was exothermic. In contrast, ketorolac binding to hIFABP was endothermic and entropy–driven. The X–ray crystal structure of DAUDA–hIFABP revealed a FA–like binding mode where the carboxylate of DAUDA formed a network of hydrogen bonds with residues at the bottom of the binding cavity and the dansyl group interacted with residues in the portal region. In contrast, NMR chemical shift perturbation (CSP) data suggested that ANS bound only towards the bottom of the hIFABP cavity, whereas ketorolac occupied only the portal region. The CSP data further suggested that ANS and ketorolac were able to bind simultaneously to hIFABP, consistent with the lack of displacement of ANS observed by fluorescence and supported by a model of the ternary complex. The NMR solution structure of the ketorolac–hIFABP complex therefore describes a newly characterized, hydrophobic ligand binding site in the portal region of hIFABP.

Intracellular lipid binding proteins (iLBPs) are low molecular weight proteins (14–15 kDa) that bind to poorly water–soluble molecules in the cytoplasm.(*1*) Fatty acid binding proteins (FABPs) are a class of iLBPs that are predominantly involved in binding, solubilization and transport of saturated and unsaturated fatty acids (FA). Nine different subtypes of FABPs share identical gene structure (4 exons separated by 3 introns) and have conserved three dimensional structures, but differ in amino acid sequence and tissue specific expression.(*2*) In spite of their differences, FABPs retain the ability to bind long chain fatty acids (LCFA) within an enclosed cavity that is composed of 10 antiparallel β–strands and is capped by a helix–turn–helix lid. Several structures of FAs bound to different subtypes of FABPs have been reported.(*3-6*) Liver FABP (LFABP) binds 2 FA molecules, whereas other FABP: ligand structures reveal 1:1 binding stoichiometry. The structures described for FABP:FA complexes differ in the orientation of the FA in the complex, but each describes a well–defined FA–binding pocket deep inside the β–barrel of the FABP.(*7*) These FABP:FA interactions are stabilized by an ionic interaction between the carboxyl terminal of the LCFA and a conserved arginine side chain and water molecules present inside the β–barrel of FABPs.(*8*) For example the electrostatic interaction of the LCFA carboxylate occurs with Arg106 in intestinal FABP (IFABP) and with Arg126 in LFABP and adipocyte FABP (AFABP) or analogues of these arginine residues within the β–barrel of other FABPs.(*6, 9, 10*) These ionic interactions appear to be largely responsible for the unique positioning of FA in different FABPs.

In addition to FAs, FABPs interact with a range of other lipophilic compounds. Binding of non–FA ligands to FABPs has been exemplified by their ability to displace bound fluorescent probes such as 11–dansylamino undecanoic acid (DAUDA) and 1–anilinonapthalene 8–sulfonic acid (ANS) from FABP.(*11, 12*) Although there is limited structural information on the binding sites of these fluorophores within the different FABPs, they have been shown to bind competitively with FA. Normally the choice of fluorophore for binding assays of this type is based on the affinity of the fluorophore for FABP and the observed change in emission spectra on binding. Using an ANS displacement assay, rat IFABP (rIFABP) has been shown to bind a range of different lipophilic drug molecules.(*11, 13*) Subsequent studies have shown that drug binding to rIFABP may promote drug absorption into the enterocyte *in vivo*

and may also reduce the intracellular free fraction available for gut wall metabolism of these ligands.(*14*) The structure of rIFABP has been reported in complex with palmitate and oleate and the structures reveal similar binding interactions with each FA.(*4, 9, 15*) This has been confirmed by single point mutation studies.(*16, 17*) These structural studies suggest no major conformational change occurs in rIFABP upon binding to a range of FAs. In contrast, AFABP has been shown to undergo a conformational change following interaction with specific ligands, and this has been suggested to promote nuclear localization and to play an important role in the ability of ligands such as FAs to interact with nuclear targets such as nuclear hormone receptors.(*18*)

Human IFABP (hIFABP) shares 82% sequence identity with rIFABP and is presumed to interact with its ligands in a similar way to rIFABP.(*19*) To this point, however, structural details of hIFABP–ligand complexes have not been reported. NMR structures of the two allelic variants of hIFABP (PDB: 3IFB and 1KZX) with either an alanine or a threonine residue at 54 have been reported.(*20, 21*) Binding data for these polymorphs of hIFABP shows a two–fold difference in their affinity towards LCFAs.(*22*) Likewise, analysis of the ligand binding properties of single point mutants of rIFABP has revealed that the mutation I23A results in significant changes in binding affinity for different LCFA.(*23*) In hIFABP, the Ile23 of rIFABP is replaced by Val and inside the β–barrel binding cavity, Ala104 of rIFABP is replaced by Thr104 in hIFABP. The effect of these substitutions on the ligand binding ability of hIFABP has not been investigated in detail.

We present in this study a detailed analysis of the structure of *apo* hIFABP and structural data on ligand binding to hIFABP and its effects on protein conformation. The ligand binding specificity of hIFABP was investigated using a range of compounds including fluorophores (i.e. ANS and DAUDA) and lipophilic drug molecules, and via a number of techniques including fluorescence displacement, isothermal titration calorimetry (ITC), NMR spectroscopy and X–ray crystallography. The ligand binding properties of hIFABP were first analyzed using fluorophore displacement assays. In this, ketorolac, a non–steroidal anti–inflammatory drug, showed low micromolar affinity for hIFABP via displacement of DAUDA but did not displace ANS. The thermodynamic signature of ketorolac binding as determined by ITC also indicated endothermic, entropy–driven binding, in contrast with the

enthalpy–driven binding of most other ligands that were tested. We subsequently elucidated the DAUDA–hIFABP complex structure by X–ray crystallography, and conducted NMR studies of ANS binding by chemical shift perturbation (CSP). These data confirm that DAUDA binds to hIFABP in a similar location to LCFA and suggest that ANS binds in a location at the bottom of the β–barrel. In contrast, 2D [^{15}N, ^{1}H]–HSQC NMR data indicate that ketorolac binds at a distinct site on hIFABP. The solution structure of the hIFABP–ketorolac complex reveals that although ketorolac is a heterocyclic carboxylic acid derivative and therefore has some FA–like features, it binds to hIFABP in a different location compared to FA and its carboxylate group fails to make any interaction with conserved arginine residues that are characteristic of FA binding. This additional binding mode may broaden the repertoire of lipophilic drugs that can bind to hIFABP, which has the potential to impact their absorption, intracellular disposition and metabolism.

RESULTS AND DISCUSSION

Selection of fluorescent probe. Ligand binding to rIFABP using ANS as a fluorescent probe has been previously investigated.(*11*) ANS binds to rIFABP with a K_D of 7.3 μM. Here we observed that ANS has a 4–fold lower binding affinity for hIFABP (K_D 31.3 μM). This renders ANS less suitable as a probe for ligand binding studies for hIFABP since a far higher concentration of ANS is required to achieve a similar binding occupancy. Consequently an alternate fluorophore, DAUDA, was investigated and found to bind with higher affinity to hIFABP (K_D 0.3 μM) and to have comparable affinity for rIFABP (K_D 0.7 μM). Figure 1 shows the fluorescence emission spectra and binding curves generated upon ANS and DAUDA binding to hIFABP. The higher affinity observed for DAUDA binding to hIFABP when compared to ANS has also been reported previously for rLFABP (DAUDA: 0.7 μM, ANS: 3.4 μM) and hLFABP (DAUDA, 0.15 μM; ANS, 6 μM).(*24-26*) Both ANS and DAUDA have been used as fluorescent probes for binding to FABP and both are displaced by FA binding.

Ligand binding affinity for hIFABP. The affinities of several ligands for hIFABP were determined using DAUDA as a fluorescent probe. Ligand binding affinities (K_i) for a range of drugs were determined by measuring their ability to displace DAUDA from the hIFABP binding cavity. The calculated K_i (μM) values of different ligands in the presence of hIFABP (via DAUDA displacement), and the values previously reported for rIFABP using the same ligands (via ANS displacement) are summarized in Table 1. The majority of these ligands showed similar affinities for the two proteins with two– to ten–fold differences in their calculated K_i values. This was not unexpected as rIFABP and hIFABP share a conserved three–dimensional structure and share 82% sequence identity. However, a notable exception was observed with ketorolac, which had a greater than 230–fold difference in affinity for rIFABP (K_i 2300 μM) when compared to hIFABP (K_i 9.4 μM). In order to determine the importance of the choice of fluorescent probe on the measured affinity, the interaction between ketorolac and hIFABP was investigated using ANS displacement. In these experiments ketorolac failed to displace ANS from the hIFABP–ANS complex. In contrast, DAUDA was completely displaced from the hIFABP–DAUDA complex by ketorolac (Figure 2). The failure of ketorolac to displace ANS was unexpected as it was assumed that ANS and DAUDA bound in a similar fashion within the cavity of

hIFABP. As such it was anticipated that ketorolac would be able to displace ANS from hIFABP as has previously been demonstrated with rLFABP.(*12*) Taken together the data suggested that the ketorolac binding site on hIFABP overlaps with that of DAUDA, but that ketorolac and ANS occupy different binding sites within the cavity of hIFABP.

Thermodynamic signatures of hIFABP binding. Isothermal titration calorimetry (ITC) was employed to better understand the different modes of ligand binding to hIFABP (Table 2). ITC has previously been used to determine the thermodynamics and stoichiometry of ligand binding for number of FABPs.(*8*) For example, ITC analysis of FAs binding to rIFABP reveals favorable enthalpies of binding, consistent with an extensive network of hydrogen bonding interactions in the complex that have been identified by structural studies.(*8*) The thermodynamic signatures of lipophilic drug binding to hIFABP, however, have not been reported.

The thermodynamic binding parameters for a range of compounds binding to hIFABP are summarized in Table 2. The ITC data obtained upon titration of hIFABP with ANS, DAUDA and ketorolac are shown in Figure 3. Individual titration data for the remainder of the compounds tested are shown in the Supplementary Figure S3. Except for fenofibric acid (N: 1.7), all of the ligands showed the expected binding stoichiometry of 1:1 with hIFABP. For fenofibrate, binding to hIFABP was observed using NMR titration studies (Supplementary Figure S4), but due to its poor aqueous solubility, fenofibrate binding could not be measured by ITC.

The binding affinities calculated by ITC and fluorescence assays were comparable for DAUDA (K_D = 0.36 μM and 0.3 μM, respectively) and ANS (K_D = 13.3 μM and 31.1 μM, respectively) (Tables 1 and 2). However, a larger difference was observed for ketorolac (K_D = 56.7 μM and 9.4 μM). This may be the result of the different buffer conditions used for the different techniques. For the two fluorophores, in addition to the measured 36–fold difference in affinity, there were notable differences in their thermodynamic binding signatures. Thus, DAUDA binding was characterized by a large favorable enthalpy change (ΔH = –11.5 ± 1.01 kcal mol^{-1}) and a small, unfavorable, entropy change ($T\Delta S$ = –2.38 ± 1.04 kcal mol^{-1}). In contrast, for ANS, approximately equal contributions to binding were observed from the changes in enthalpy and entropy (ΔH = –3.66 ± 0.39 kcal mol^{-1}; $T\Delta S$ = 3.28 ± 0.52 kcal mol^{-1}).

The thermodynamic signature of the ketorolac–hIFABP interaction was distinct from all of the other compounds tested, since the enthalpy change on binding of ketorolac to hIFABP was endothermic and was observed as positive peaks in the raw ITC data (Figure 3). Thus the binding of ketorolac to hIFABP was entropy–driven and the entropy change on binding was larger than for any of the other compounds tested ($T\Delta S$ = 6.09 ± 0.04 kcal mol^{-1}). Only fenofibric acid showed a similarly favorable entropy change on binding ($T\Delta S$ = 6.04 ± 0.47 kcal mol^{-1}).

The large and favorable enthalpy change that has been reported previously upon binding of FA to FABP is thought to arise from the network of hydrogen bonds formed between the carboxylate head group of the FA and residues in the cavity of the protein.(*9*) For example, oleic acid has been reported to bind to rIFABP with high affinity (K_D = 27 nM) and the binding is enthalpically favorable (ΔH = –11 ± 1 kcal mol^{-1}; $T\Delta S$ = 0 ± 1 kcal mol^{-1}).(*27*) The structure of palmitate in complex with rIFABP reveals that the carboxylate head group of the FA makes hydrogen bonds to the side chains of Arg106 and Trp82 within the protein.(*9, 17*) Similar thermodynamic profiles for other LCFA binding to rIFABP suggest a similar mode of binding.(*27*) Mutation of R106A results in a less favorable enthalpy change with a reduction of ~4 kcal mol^{-1} observed on binding of oleic acid, consistent with the loss of hydrogen bonding. However, somewhat surprisingly, the loss of enthalpy is more than compensated for by a favorable entropy change in the R106A mutant and oleic acid was observed to bind with increased affinity to the mutant (K_D = 2 nM).(*23*) It appears, therefore, that high–affinity interactions with IFABP can be achieved by different modes of binding and that the thermodynamic signatures may reflect these different binding modes. In light of this, we sought to structurally characterize the binding of DAUDA, ANS (both as examples of enthalpic binders and to investigate the modes of binding of these fluorescent probes) and ketorolac (as an entropic binder) to hIFABP. In the case of DAUDA, we were able to obtain co-crystals of the complex with hIFABP.(*28*) Similar attempts to generate co-crystals of ketorolac and ANS were unsuccessful, and therefore these complexes were characterized using NMR spectroscopy.

Chemical Shift Perturbation (CSP) mapping of binding interactions. The inability of ketorolac to displace ANS in the fluorescence assays suggested that they may occupy different sites in the binding cavity of hIFABP. In order to define the binding modes for ketorolac and ANS we first undertook NMR chemical shift perturbation

(CSP) studies by monitoring changes in the 2D [^{15}N, ^{1}H]–HSQC spectra of the ^{15}N–labeled protein. First, a series of titrations were performed by addition of increasing concentrations of either ANS or ketorolac to ^{15}N–labeled hIFABP. CSP were calculated by comparing the *holo* spectra resulting from increasing ligand additions, with the *apo* spectrum. This enabled identification of the residues in hIFABP that were perturbed by each ligand. Subsequently, a ^{15}N–labeled hIFABP sample, saturated with ANS, was titrated with ketorolac. The chemical shifts of hlFABP were assigned using standard 2D and 3D NMR techniques as described in the methods section and the assignments have been deposited in the BMRB (19727). The CSPs generated from these experiments are depicted in Figure 4A. Addition of ANS to a final concentration of 250 μM resulted in CSP of > 0.1 ppm for 34 cross peaks in the spectrum. In addition, several residues were broadened beyond the limit of detection. This is consistent with ANS being in intermediate exchange on the NMR timescale. Addition of ketorolac to a final concentration of 2.5 mM resulted in CSP > 0.1 ppm for 38 cross peaks. In each case, the perturbed residues were mapped onto the *apo* NMR structure of hIFABP (PDB: 3IFB) and the results are depicted in Figure 4B. As shown in Figure 4B, the residues perturbed by ketorolac mapped onto both α–helices, the adjacent hairpins of the β–sheets and the loop regions that are all located in the portal region of hIFABP. Conversely, the mapping of residues perturbed by ANS was more consistent with binding deep inside the β–barrel of hIFABP. Only ten residues (N24, A32, D34, S52, F93, T96, Q115, Y117, A124, and K125) with CSPs > 0.1 ppm were found to be common to both ANS and ketorolac titrations, indicating little overlap of their binding sites. Most of these residues were located in the middle of the β strands, consistent with their location at the intersection of the ANS and ketorolac binding sites. Addition of ketorolac to a sample of hIFABP that had been saturated with ANS resulted in CSP of > 0.1 ppm being observed in spectra of the mixture for residues that are perturbed only by ANS (G22, K27, K29, L30, A31, A54, F55, E77, G80 and T104) and residues that are perturbed only by ketorolac (S4, K7, D9, E12, V66, T67, W82, L89, G91 and K129). The extent of the CSPs observed in the presence of both ligands is consistent with hIFABP binding both ligands simultaneously (Figure 4A).

Binding of ANS resulted in a large perturbation of the backbone amide cross peak of Trp82 (CSP: 0.18 ppm) and broadening of the amide side chain (Hε/Nε) peak of

Arg106. These residues form hydrogen bonds with the carboxylate of FA in crystal structures of their complexes with hIFABP. The perturbation of these residues in the 2D [^{15}N,^{1}H]–HSQC spectrum, the overall pattern of CSP observed upon titration of hIFABP with ANS and the favorable enthalpy of binding observed for ANS by ITC are consistent with the sulfonate moiety of ANS forming similar polar contacts upon binding to hIFABP.

Structures have previously been reported for ANS in complex with human heart FABP (hHFABP) and mouse AFABP (mAFABP) (PDB: 2ANS).(*29, 30*) In each case, ANS was found to bind in the portal region of the protein. This mode of binding is not consistent with the pattern of CSP induced by ANS binding to hIFABP in the current study. However, IFABP has also been observed to bind FA in a manner distinct from HFABP and AFABP. IFABP binds FA in a slightly bent conformation with the carboxylate buried deep in the protein cavity and directly coordinated to Arg106, whereas HFABP and AFABP bind FA in a U–shaped conformation with the carboxylate head group coordinated to Arg126.(*5, 6*) Thus, the different mode of binding observed for ANS binding to hIFABP is in line with the different binding modes that have been observed with FA.

Structural analysis of the ketorolac–hIFABP complex by NMR. To characterize the binding site for ketorolac in hIFABP, we determined a structure for the complex using NMR spectroscopy. Sequence–specific ^{1}H, ^{13}C and ^{15}N assignments were obtained for ketorolac–bound hIFABP using standard 2D and 3D NMR experiments. Due to line broadening some resonances were not observed. These included the amide resonances of Ala73, Arg79 and Val105 and C$^{\alpha}$ and C$^{\beta}$ resonances for Phe55 and Tyr70. No resonances were observed for Arg56, Asn71 and Leu72. Assignments for ketorolac in the absence of protein were made using standard 1D and 2D NMR experiments in hIFABP sample buffer and only small changes in the chemical shifts were observed in the hIFABP bound sample (Supplementary Figure S5). The position of ketorolac in the complex was calculated using 30 unambiguous intermolecular NOEs that were observed in NOESY experiments (Supplementary Table S2). Structures for the complex were generated using standard NOE–based approaches for structure calculation and refinement in CNS as described. The solution structure of hIFABP in complex with ketorolac contains the 10–stranded β–barrel capped by helix–turn–helix lid that is characteristic of members of the FABP

family. The structure is well–defined, with an RMSD of 0.55 Å and 1.03 Å for the backbone atoms and the heavy atoms of the whole protein (residues: 1–131), respectively. The structure statistics, including the RMSD values and constraint violations are listed in Supplementary Table S3. A family of 10 conformers with the lowest energy were selected after refinement and the ensemble of these structures is shown in Figure 5A.

Overall, the solution structure of hIFABP–ketorolac is well defined except in the portal region including the hairpin loop regions (β_{CD} and β_{EF}), the helix–turn–helix and the loop connecting αII to strand βB (Figure 5A). Binding of ketorolac induces chemical exchange broadening of the NMR resonances of several residues in these regions preventing their chemical shift assignment. In particular the hairpin turn β_{EF} located opposite to the helix–turn–helix lid was the least well–defined owing to a lack of assignments in the NMR data. The helix–turn–helix lid shows the greatest conformational change upon binding with ketorolac, when compared with the *apo* structure of hIFABP (PDB: 3IFB).(*21*) After superposition of this *apo*–structure and the ketorolac–hIFABP complex, the displacement of residues revealed a movement of 7.6 Å in helix αII, (measured between the positions of the C^{α} of Ile25), 2.1 Å in helix αI (measured between the positions of the C^{α} of Met18) and 2.8 Å to 5.8 Å in the loop between the two helices (measured between the positions of the C^{α} of Gly22 and Asn24, respectively).

These conformational changes are supported by both intra– and inter–molecular NOEs. Specifically, intramolecular NOEs observed between the residues of helix αI (Y14–M21), residues of the hairpin loops β_{IJ} (Y119–V122) and βJ (A124–K125) are consistent with the closed conformation observed in the complex. Furthermore, intermolecular NOEs observed between residues of helix αI (Phe17, Met18, and Met21), the helix–turn–helix loop (Val23) and ketorolac suggest that direct contacts with the ligand are partly responsible for stabilizing the closed conformation (Supplementary Table S2). The conformational changes in the portal region of hIFABP upon binding to ketorolac are consistent with previous observations of backbone dynamics in a similar region of *apo* hLFABP that are stabilized by FA binding.(*31*)

The position of ketorolac in the portal region of hIFABP is well defined in all of the 10 conformers using 30 intermolecular NOEs (Supplementary Table S2). The position of ketorolac binding is consistent with the patterns of CSP observed in the 2D [^{15}N,^{1}H]–HSQC spectra. Ketorolac is located in a binding site adjacent to the portal of hIFABP and appears to be stabilized by hydrophobic interactions in this region. The carboxylate of ketorolac points towards the bottom of the β–barrel, but is separated by > 7 Å from the guanidinium group of Arg106 and there are no polar interactions evident between ketorolac and Arg106 in any of the conformers. Although the carboxylate was located closer to Arg126, it was separated by more than 4.3 Å and no polar contacts were observed. In five of the conformers a polar contact was identified between the carbonyl oxygen of ketorolac and the hydroxyl of the Tyr70 side chain. The binding site, defined as the residues located within 4 Å of ketorolac in the complex, is shown in Figure 5B. Ketorolac is enclosed mainly by hydrophobic residues. Thus the phenyl ring is surrounded by M18, M21, V23, K27, I58, Y70 and L78 whilst the pyrollizine ring is adjacent to Y14, F17, F93, L102, and Y117. These residues make extensive nonpolar contacts with ketorolac consistent with the entropy–driven binding determined by ITC. Therefore, although ketorolac contains a carboxylate moiety, it appears to bind in the cavity of hIFABP in an environment distinct to that of FA, and in a mode driven largely by hydrophobic rather than electrostatic or polar interactions.

Structural analysis of the hIFABP–DAUDA complex. The ability of ketorolac to displace DAUDA from the hIFABP binding cavity is consistent with the two ligands having overlapping binding sites. Details of the crystallization and preliminary X–ray diffraction data for the hIFABP–DAUDA complex have been previously described.(*28*) Herein we present details of the structure of the hIFABP–DAUDA complex. Crystals of the complex diffracted beyond 1.9 Å and four copies of hIFABP were found to be present in the asymmetric unit. Each of these four hIFABP monomers had one molecule of DAUDA bound in the FA–binding cavity (Supplementary Figure S1B). The individual monomers of hIFABP were superimposed over chain A (Supplementary Figure S1A) with an average root mean square deviation (RMSD) of 0.3 Å (all atoms). Chain C had the highest RMSD of 0.36 Å compared with the other chains. For simplicity, and due to the similarity observed in each of the four monomers we restrict our discussion to chain A of

hIFABP. A summary of X–ray data processing and refinement statistics is given in Supplementary Table S1.

Superimposition of the hIFABP crystal structure and the hIFABP NMR structure (PDB: 3IFB) resulted in an average backbone RMSD of 1.58 Å. Siginificant differences were observed in the strands β_{CD} and hairpin loops in the portal region of hIFABP where the dansyl group of DAUDA was located. Otherwise only small differences between the two structures were observed between *apo* and *holo* protein. The hIFABP–DAUDA complex structure showed five internal ordered water molecules in the β–barrel cavity. As there is no crystal structure of *apo*–hIFABP, it is not possible to compare the exact number and placement of these water molecules in the complex structure. A Mg^{2+} ion was also observed in the binding cavity, although it made no specific interactions with either hIFABP or DAUDA. The significance of this ion is not clear and is most likely an artefact of the crystallization conditions, which contained 0.2 M $MgCl_2$.

DAUDA, which consists of a 5–N–dimethyl amino napthalene head group connected to a long FA chain, bound to hIFABP in an elongated fashion, with the FA chain adopting a bent geometry. The carboxylate group of DAUDA formed hydrogen bonds with side chains of Trp82 and Arg106 at the bottom of the binding cavity of hIFABP (Supplementary Figure S2). The hydrogen bonding of the DAUDA tail with these particular residues is equivalent to that observed for FAs interacting with rIFABP, which fixes their position deep inside the β–barrel cavity.(*9*) An additional hydrogen bond was also observed between the sulfonamide nitrogen of DAUDA and the side chain hydroxyl of Tyr14 (Supplementary Figure S2). The DAUDA FA chain resides in a crevice formed by hydrophobic and aromatic side chains of hIFABP, and this interacts with the “convex” face of the DAUDA molecule. The bent geometry of the FA chain of DAUDA is similar to that observed for FA binding to rIFABP.(*9*) The head group of DAUDA lies parallel to the helix–turn–helix lid of hIFABP, and residues in the hairpin loops of β_{CD} and β_{EF} which are perturbed to accommodate this bulky group. Due to the large size and elongated conformation of the DAUDA molecule, it fits simultaneously inside the deep β–barrel cavity and in the portal region of hIFABP. The structure reveals that DAUDA forms an extensive network of interactions with hIFABP which explains the high binding affinity for hIFABP and is consistent with the enthalpically favorable binding observed by ITC.

Superimposing the structures of DAUDA–hIFABP with ketorolac–hIFABP (Figure 7A) clearly showed that the dansyl group of DAUDA and ketorolac both occupy the portal region of hIFABP. However, the conformations of the helix–turn–helix lid and the portal hairpin loops in DAUDA– and ketorolac–bound hIFABP are quite distinct from each other. Binding of DAUDA resulted in an open conformation whereas binding of ketorolac stabilized the closed conformation of this lid. Measurement of distances between equivalent residues in the two structures reveals a displacement of 7.6 Å in helix αII (measured between C^{α} of Ile25). These structural data reveal the overlapping binding sites of DAUDA and ketorolac and explain the ability of ketorolac to displace DAUDA from the hIFABP complex.

Docking model of the ternary hIFABP–ketorolac–ANS complex. A model of the ternary complex of ketorolac and ANS bound to hIFABP was generated by induced fit docking using Glide.(*32*) The ANS was docked into hIFABP–ketorolac complex using CSP observed in the NMR experiments as restraints. The seven models of the complex having the highest Glide scores are depicted in Figure 7B. The modelling reveals that both ligands can be accommodated simultaneously within the binding cavity of hIFABP. Only minor changes to the conformation of the protein or the location of ketorolac were observed in the ternary complex in comparison to the NMR–derived model of the binary complex with ketorolac. This model is consistent with the lack of displacement observed in the fluorescence experiments and the CSP data for both the individual ligands and the ternary complex.

Conclusion

In this study, we have characterized a previously unreported binding site for small molecules on hIFABP by the application of several biophysical techniques (fluorescence, ITC, solution NMR spectroscopy and X–ray crystallography). The study reveals that hIFABP is able to bind to different lipophilic compounds at two different sites and via different modes of interaction. Binding at the FA site appears to be driven by polar interactions with residues at the bottom of the hIFABP cavity and is characterized by favorable binding enthalpy. In contrast, binding at the portal site is dominated by hydrophobic interactions and appears to be largely entropy driven.

The biophysical binding data for ketorolac binding to hIFABP suggest that this complex is likely to be formed in the enterocyte. After oral administration of ketorolac (1.7 mg kg^{-1}), plasma concentrations of up to 10 μg ml^{-1} (~40 μM) have been reported, which is similar to the K_D value that we have measured for ketorolac binding to hIFABP in the current study.(*33*) Although intracellular drug concentrations have not been reported, the concentration of ketorolac in the enterocyte during absorption is likely to be significantly higher than the observed plasma concentrations. Since hIFABP may constitute as much as 1–2% of the cytosolic protein in enterocytes, it is likely that ketorolac binding to hIFABP is significant.(*34*) The consequences of this interaction in terms of absorption, intracellular distribution and metabolism of ketorolac are currently unknown, although previous studies have shown that drug binding to FABP may promote entry into the enterocyte and reduce the prevalence of enterocyte based metabolism.(*14*)

There is increasing evidence that several iLBPs including FABP are able to bind lipophilic ligands, including endogenous molecules and drugs. Furthermore, binding to FABP has been demonstrated to influence the partitioning of some drugs within cells and their ability to bind to intracellular targets.(*35-37*) Many of the drugs that bind FABP contain carboxylate functional groups, suggesting that they may bind in a similar manner to FA.(*12, 38*) However, the presence of a second binding site in hIFABP, which is able to bind ligands via hydrophobic interactions, raises the possibility that the binding repertoire of hIFABP may be broader than currently recognized. The presence of a second ligand binding site in LFABP, which is able to bind ligands via largely hydrophobic interactions, is thought to be responsible in part for its broad ligand binding specificity.(*3, 31, 39*) The consequences of binding to the hydrophobic portal site of hIFABP on ligand distribution and receptor activation within cells is the subject of ongoing investigations.

METHODS

Full details of the materials and methods used in this study are outlined in the Supplementary Information.

ASSOCIATED CONTENT

Supplementary Information

This section contains details of Methods, Tables, and Figures as indicated in the text. This material is available free of charge via the Internet at http://pubs.acs.org.

Accession Codes

Chemical shifts of hIFABP in complex with ketorolac have been deposited in BMRB, with the accession number 19727, and the coordinates of the complex in the PDB, accession number 2MJI. The crystal structure of hIFABP–DAUDA has been deposited in the PDB, accession number 3AKM.

AUTHOR INFORMATION

Corresponding Authors

* Email: Martin.Scanlon@monash.edu; Chris.Porter@monash.edu

ACKNOWLEDGMNTS

This work was supported by an Australian Research Council Discovery Grant. Rahul Patil acknowledges financial support provided by a Monash Graduate Scholarship (MGS) and Monash International Postgraduate Research Scholarship (MIPRS).

ABBREVIATIONS

FABP, fatty acid binding protein; LFABP, Liver fatty acid binding protein; AFABP, Adipocyte fatty acid binding protein; rIFABP, Rat intestinal fatty acid binding protein; hIFABP, Human intestinal fatty acid binding protein; iLBP, Intracellular lipid binding protein; ANS, 1–anilinonapthalene 8–sulfonic acid; DAUDA, 11–Dansylamino undecanoic Acid; FA, fatty acid; ITC, isothermal titration calorimetry

REFERENCES

1. Kaikaus, R. M., Bass, N. M., and Ockner, R. K. (1990) Functions of fatty acid binding proteins, *Experientia 46*, 617–630.
2. Chmurzynska, A. (2006) The multigene family of fatty acid–binding proteins (FABPs): function, structure and polymorphism, *J. Appl. Genet. 47*, 39–48.

3. Thompson, J., Winter, N., Terwey, D., Bratt, J., and Banaszak, L. (1997) The crystal structure of the liver fatty acid–binding protein. A complex with two bound oleates, *J. Biol. Chem. 272*, 7140–7150.
4. Sacchettini, J. C., Gordon, J. I., and Banaszak, L. J. (1989) Crystal structure of rat intestinal fatty–acid–binding protein. Refinement and analysis of the *Escherichia coli*–derived protein with bound palmitate, *J. Mol. Biol. 208*, 327–339.
5. Zanotti, G., Scapin, G., Spadon, P., Veerkamp, J. H., and Sacchettini, J. C. (1992) Three–dimensional structure of recombinant human muscle fatty acid–binding protein, *J. Biol. Chem. 267*, 18541–18550.
6. Marr, E., Tardie, M., Carty, M., Brown Phillips, T., Wang, I. K., Soeller, W., Qiu, X., and Karam, G. (2006) Expression, purification, crystallization and structure of human adipocyte lipid–binding protein (aP2), *Acta Cryst. F 62*, 1058–1060.
7. Furuhashi, M., and Hotamisligil, G. S. (2008) Fatty acid-binding proteins: role in metabolic diseases and potential as drug targets, *Nat. Rev. Drug Discov. 7*, 489-503.
8. Richieri, G. V., Ogata, R. T., Zimmerman, A. W., Veerkamp, J. H., and Kleinfeld, A. M. (2000) Fatty acid binding proteins from different tissues show distinct patterns of fatty acid interactions, *Biochemistry 39*, 7197-7204.
9. Sacchettini, J. C., Scapin, G., Gopaul, D., and Gordon, J. I. (1992) Refinement of the structure of *Escherichia coli*-derived rat intestinal fatty acid binding protein with bound oleate to 1.75–A resolution. Correlation with the structures of the apoprotein and the protein with bound palmitate, *J. Biol. Chem. 267*, 23534–23545.
10. Sharma, A., and Sharma, A. (2011) Fatty Acid Induced Remodeling within the Human Liver Fatty Acid–binding Protein, *J. Biol. Chem. 286*, 31924–31928.
11. Velkov, T., Horne, J., Laguerre, A., Jones, E., Scanlon, M. J., and Porter, C. J. H. (2007) Examination of the role of intestinal fatty acid–binding protein in drug absorption using a parallel artificial membrane permeability assay, *Chem. Biol. 14*, 453–465.
12. Chuang, S., Velkov, T., Horne, J., Porter, C. J. H., and Scanlon, M. J. (2008) Characterization of the drug binding specificity of rat liver fatty acid binding protein, *J. Med. Chem. 51*, 3755–3764.

13. Velkov, T., Lim, M. L., Horne, J., Simpson, J. S., Porter, C. J., and Scanlon, M. J. (2009) Characterization of lipophilic drug binding to rat intestinal fatty acid binding protein, *Mol. Cell. Biochem. 326*, 87–95.
14. Trevaskis, N. L., Nguyen, G., Scanlon, M. J., and Porter, C. J. (2011) Fatty acid binding proteins: potential chaperones of cytosolic drug transport in the enterocyte?, *Pharm. Res. 28*, 2176–2190.
15. Hodsdon, M. E., Ponder, J. W., and Cistola, D. P. (1996) The NMR solution structure of intestinal fatty acid–binding protein complexed with palmitate: application of a novel distance geometry algorithm, *J. Mol. Biol. 264*, 585–602.
16. Jakoby, M. G., Miller, K. R., Toner, J. J., Bauman, A., Cheng, L., Li, E., and Cistola, D. P. (1993) Ligand–protein electrostatic interactions govern the specificity of retinol– and fatty acid–binding proteins, *Biochemistry 32*, 872–878.
17. Eads, J., Sacchettini, J. C., Kromminga, A., and Gordon, J. I. (1993) *Escherichia coli*–derived rat intestinal fatty acid binding protein with bound myristate at 1.5 A resolution and I–FABPArg106—>Gln with bound oleate at 1.74 A resolution, *J. Biol. Chem. 268*, 26375–26385.
18. Gillilan, R. E., Ayers, S. D., and Noy, N. (2007) Structural basis for activation of fatty acid–binding protein 4, *J. Mol. Biol. 372*, 1246–1260.
19. Lowe, J. B., Boguski, M. S., Sweetser, D. A., Elshourbagy, N. A., Taylor, J. M., and Gordon, J. I. (1985) Human liver fatty acid binding protein. Isolation of a full length cDNA and comparative sequence analyses of orthologous and paralogous proteins, *J. Biol. Chem. 260*, 3413–3417.
20. Zhang, F., Lucke, C., Baier, L. J., Sacchettini, J. C., and Hamilton, J. A. (2003) Solution structure of human intestinal fatty acid binding protein with a naturally–occurring single amino acid substitution (A54T) that is associated with altered lipid metabolism, *Biochemistry 42*, 7339–7347.
21. Zhang, F., Lucke, C., Baier, L. J., Sacchettini, J. C., and Hamilton, J. A. (1997) Solution structure of human intestinal fatty acid binding protein: implications for ligand entry and exit, *J. Biomol. NMR 9*, 213–228.
22. Baier, L. J., Sacchettini, J. C., Knowler, W. C., Eads, J., Paolisso, G., Tataranni, P. A., Mochizuki, H., Bennett, P. H., Bogardus, C., and Prochazka, M. (1995) An amino acid substitution in the human intestinal fatty acid binding

protein is associated with increased fatty acid binding, increased fat oxidation, and insulin resistance, *J. Clin. Invest. 95*, 1281–1287.

23. Richieri, G. V., Low, P. J., Ogata, R. T., and Kleinfeld, A. M. (1998) Thermodynamics of fatty acid binding to engineered mutants of the adipocyte and intestinal fatty acid–binding proteins, *J. Biol. Chem. 273*, 7397–7405.
24. Norris, A. W., and Spector, A. A. (2002) Very long chain n–3 and n–6 polyunsaturated fatty acids bind strongly to liver fatty acid–binding protein, *J. Lipid Res. 43*, 646–653.
25. Maatman, R. G., van Moerkerk, H. T., Nooren, I. M., van Zoelen, E. J., and Veerkamp, J. H. (1994) Expression of human liver fatty acid–binding protein in *Escherichia coli* and comparative analysis of its binding characteristics with muscle fatty acid–binding protein, *Biochim. Biophys. Acta 1214*, 1–10.
26. Velkov, T. (2013) Interactions between Human Liver Fatty Acid Binding Protein and Peroxisome Proliferator Activated Receptor Selective Drugs, *Ppar Res. 2013*, 938401.
27. Richieri, G. V., Ogata, R. T., and Kleinfeld, A. M. (1995) Thermodynamics of fatty acid binding to fatty acid–binding proteins and fatty acid partition between water and membranes measured using the fluorescent probe ADIFAB, *J. Biol. Chem. 270*, 15076–15084.
28. Laguerre, A., Wielens, J., Parker, M. W., Porter, C. J., and Scanlon, M. J. (2011) Preparation, crystallization and preliminary X–ray diffraction analysis of two intestinal fatty–acid binding proteins in the presence of 11–(dansylamino)undecanoic acid, *Acta Cryst. F 67*, 291–295.
29. Hirose, M., Sugiyama, S., Ishida, H., Niiyama, M., Matsuoka, D., Hara, T., Mizohata, E., Murakami, S., Inoue, T., Matsuoka, S., and Murata, M. (2013) Structure of the human–heart fatty–acid–binding protein 3 in complex with the fluorescent probe 1–anilinonaphthalene–8–sulphonic acid, *J. Synchrotron Rad. 20*, 923–928.
30. Ory, J. J., and Banaszak, L. J. (1999) Studies of the ligand binding reaction of adipocyte lipid binding protein using the fluorescent probe 1, 8–anilinonaphthalene–8–sulfonate, *Biophys. J. 77*, 1107–1116.
31. Cai, J., Lucke, C., Chen, Z., Qiao, Y., Klimtchuk, E., and Hamilton, J. A. (2012) Solution structure and backbone dynamics of human liver fatty acid binding protein: fatty acid binding revisited, *Biophys. J. 102*, 2585–2594.

32. Sherman, W., Day, T., Jacobson, M. P., Friesner, R. A., and Farid, R. (2006) Novel procedure for modeling ligand/receptor induced fit effects, *J. Med. Chem. 49*, 534–553.
33. Mroszczak, E. J., Lee, F. W., Combs, D., Sarnquist, F. H., Huang, B. L., Wu, A. T., Tokes, L. G., Maddox, M. L., and Cho, D. K. (1987) Ketorolac Tromethamine Absorption, Distribution, Metabolism, Excretion, and Pharmacokinetics in Animals and Humans, *Drug Metab. Dispos. 15*, 618–626.
34. Bass, N. M., Manning, J. A., and Ockner, R. K. (1985) Turnover and short–term regulation of fatty acid binding protein in liver, *J. Biol. Chem. 260*, 9603–9607.
35. Schug, T. T., Berry, D. C., Shaw, N. S., Travis, S. N., and Noy, N. (2007) Opposing effects of retinoic acid on cell growth result from alternate activation of two different nuclear receptors, *Cell 129*, 723–733.
36. Tan, N. S., Shaw, N. S., Vinckenbosch, N., Liu, P., Yasmin, R., Desvergne, B., Wahli, W., and Noy, N. (2002) Selective cooperation between fatty acid binding proteins and peroxisome proliferator–activated receptors in regulating transcription, *Mol. Cell. Biol. 22*, 5114–5127.
37. Kraemer, F. B., and Shen, W. J. (2002) Hormone–sensitive lipase: control of intracellular tri–(di–)acylglycerol and cholesteryl ester hydrolysis, *J. Lipid Res. 43*, 1585–1594.
38. Chuang, S., Velkov, T., Horne, J., Wielens, J., Chalmers, D. K., Porter, C. J. H., and Scanlon, M. J. (2009) Probing the Fibrate Binding Specificity of Rat Liver Fatty Acid Binding Protein, *J. Med. Chem. 52*, 5344–5355.
39. Richieri, G. V., Ogata, R. T., and Kleinfeld, A. M. (1996) Thermodynamic and kinetic properties of fatty acid interactions with rat liver fatty acid–binding protein, *J. Biol. Chem. 271*, 31068–31074.

Figures

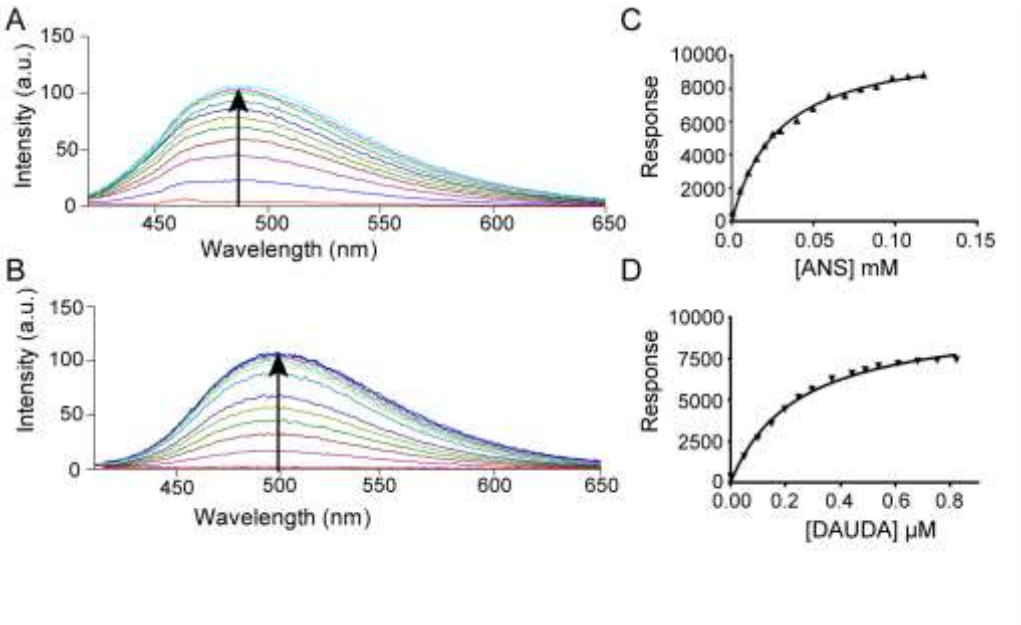

Figure 1. Fluorescence emission spectra for hIFABP following addition of increasing concentrations of (A) ANS and (B) DAUDA. The arrow indicates the direction of increasing fluorescence intensity and probe concentration. Binding curves obtained from the fluorescence titrations of (C) ANS and (D) DAUDA in the presence of hIFABP. The solid line represents the best fit to a one site binding hyperbola.

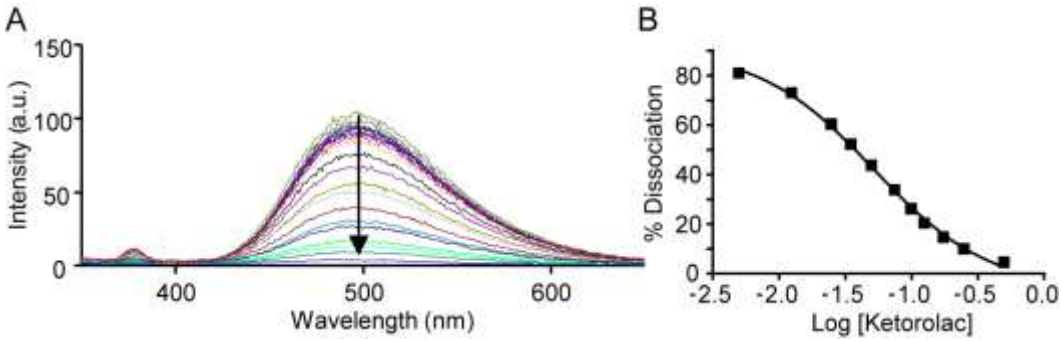

Figure 2. (A) Fluorescence emission spectra following the displacement of DAUDA from hIFABP by titration with ketorolac. The arrow represents the direction of decreasing DAUDA fluorescence with increasing ketorolac concentration. (B) Displacement curve of ketorolac competing for the DAUDA binding site of hIFABP. The solid line represents the optimal curve fitting to a one site competition model.

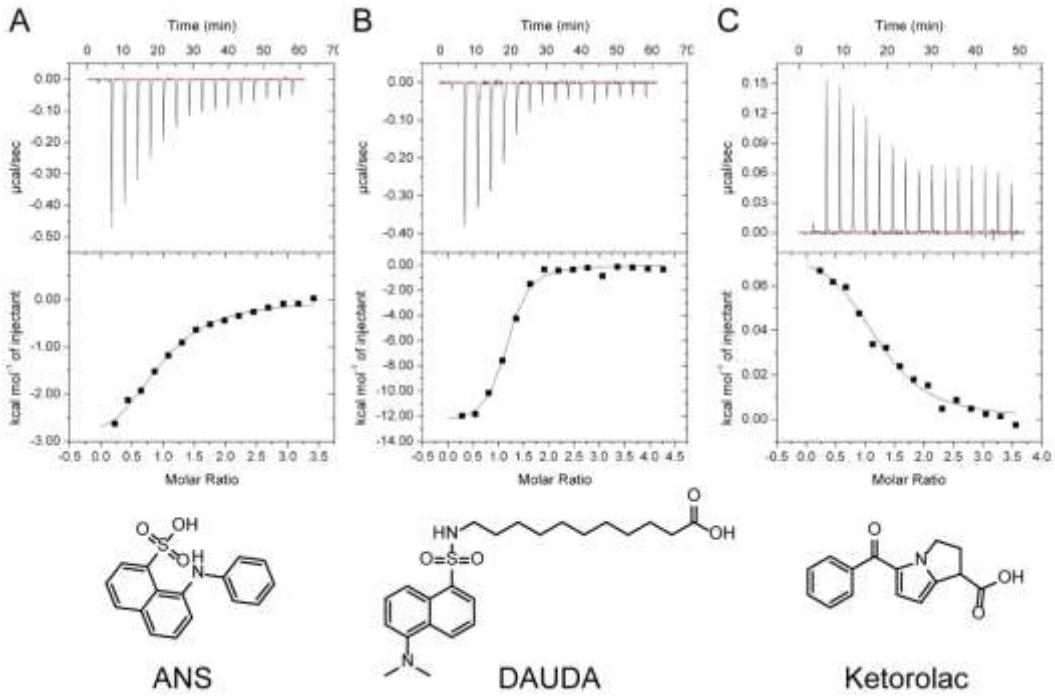

Figure 3. ITC data of compound titrations with hIFABP. The upper panels show the raw data from individual ITC experiments and the lower panels show the binding isotherm generated from the corresponding data fitted to the one-site binding site model. (A) Titration of hIFABP (50 µM) with ANS (800 µM) and, (B) Titration of DAUDA (10 µM) with hIFABP (200 µM) (due to the low solubility of DAUDA, hIFABP was titrated from the syringe in this case); and (C) Titration of hIFABP (300 µM) with ketorolac (4500 µM). All experiments were performed in triplicate at 37 °C.

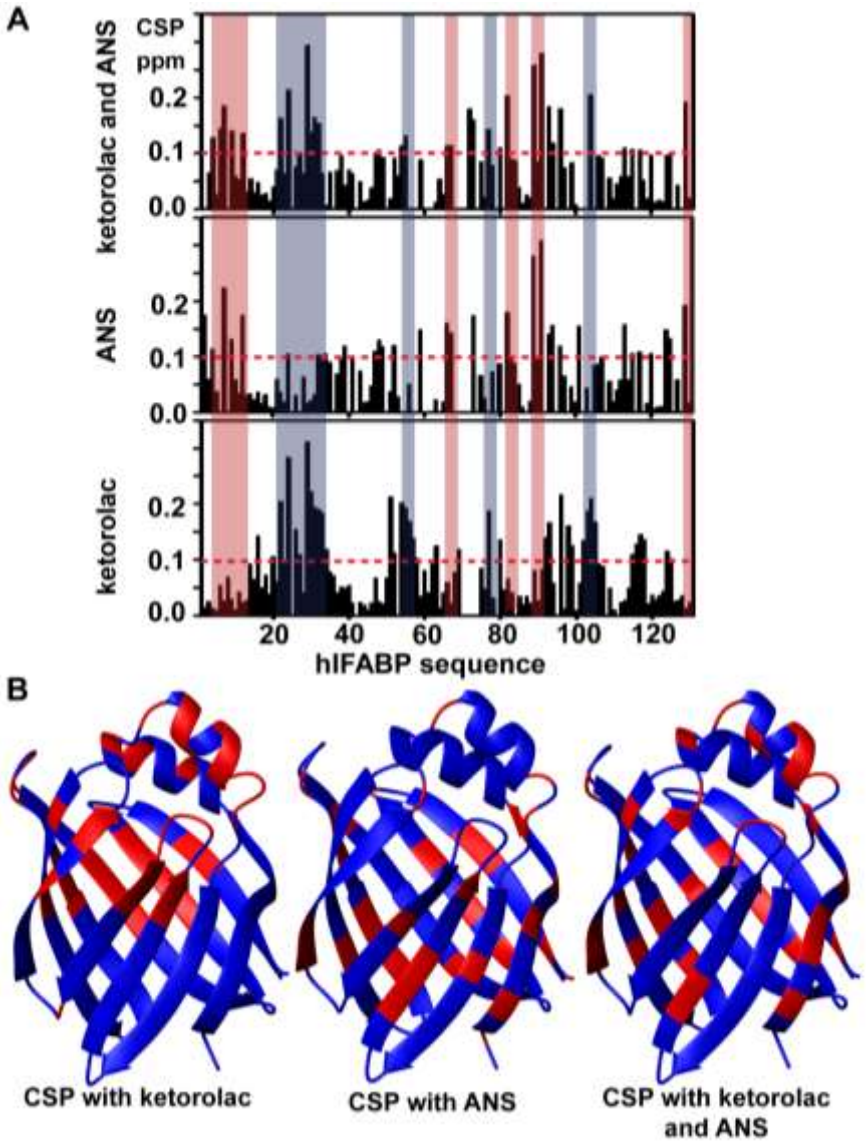

Figure 4. (A) CSP observed in HSQC spectra of hIFABP in the presence of different ligands (top panel: ^{15}N hIFABP 250 µM + ANS 250 µM + ketorolac 2.5 mM; middle panel: ^{15}N hIFABP 250 µM + ANS 250 µM; bottom panel: ^{15}N hIFABP 250 µM + ketorolac 2.5 mM). CSPs are plotted against hIFABP sequence number. The red bars highlight residues that were perturbed (> 0.1 ppm) by ANS but not ketorolac. The grey bars indicate residues perturbed (> 0.1 ppm) by ketorolac but not ANS. (B) The location of CSPs > 0.1 ppm that were observed following addition of ketorolac, ANS and both ANS and ketorolac are mapped onto the hIFABP structure (PDB: 3IFB).

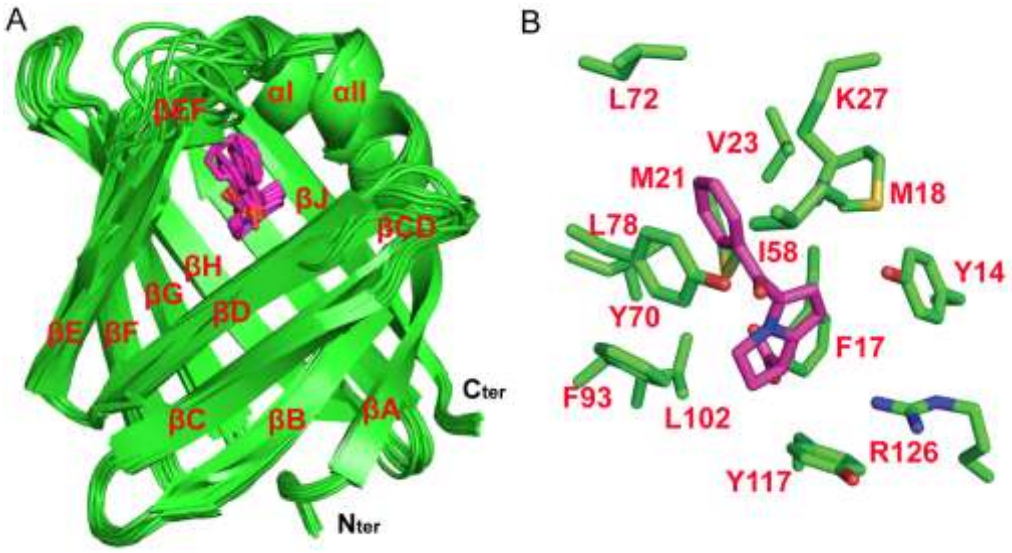

Figure 5. (A) Superimposition of the 10 conformers of hIFABP with the lowest energy, showing the regions of greatest variability (β_{CD} and β_{EF}) within the structure of the hIFABP-ketorolac complex. (B) The binding site from the conformer closest to the mean structure, showing ketorolac (in stick with magenta carbons) with residues (green carbons) located within 4Å. O, N and S shown in red, blue and yellow, respectively.

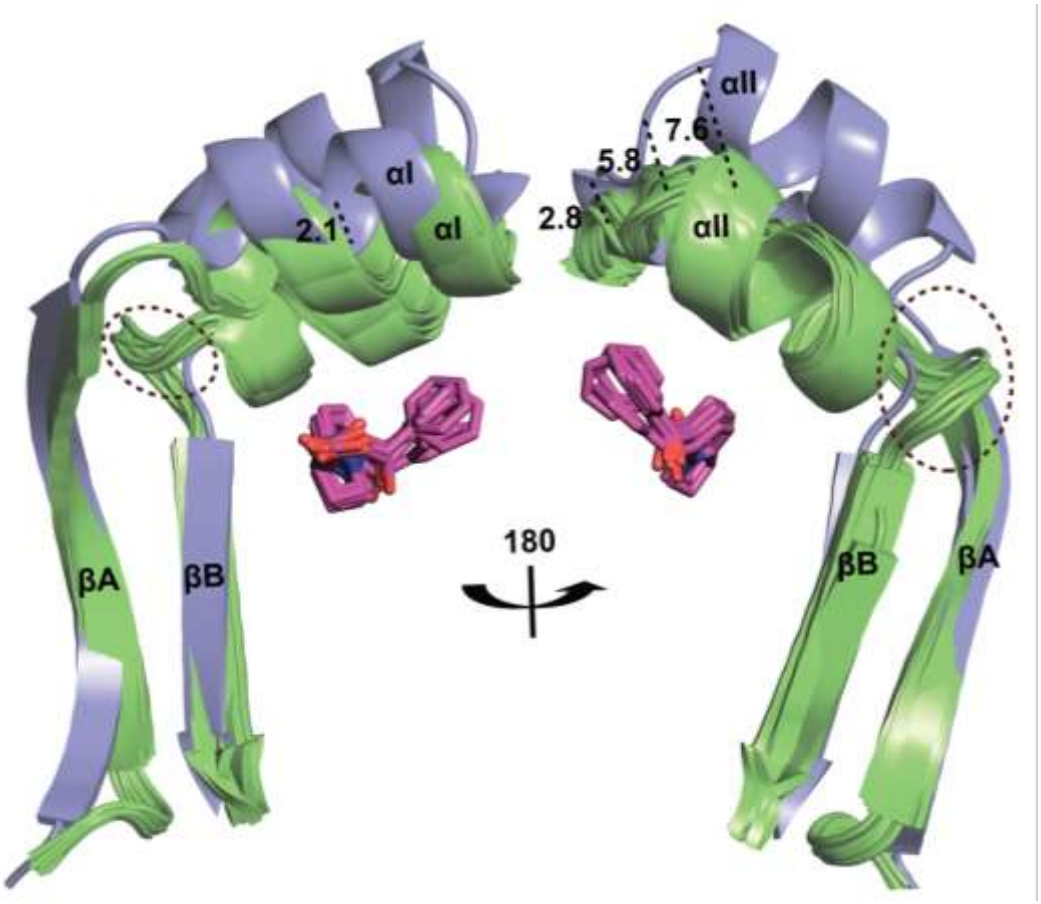

Figure 6. Change in the conformation of hIFABP upon ketorolac binding. Superimposition of hIFABP (blue) (PDB: 3IFB) and 10 conformers of hIFABP-ketorolac (green) with only αI, αII, βA, βB and connecting loops shown. Distances measured between C^{α} of Ile25 (7.6 Å), Asn24 (5.8 Å), Gly22 (2.8 Å) and Met18 (2.1 Å) between two structures are shown a dotted lines and labelled. The bend in the loop αII and βB (circled) observed the hIFABP-ketorolac complex is supported by experimental NOE-derived distance restraints.

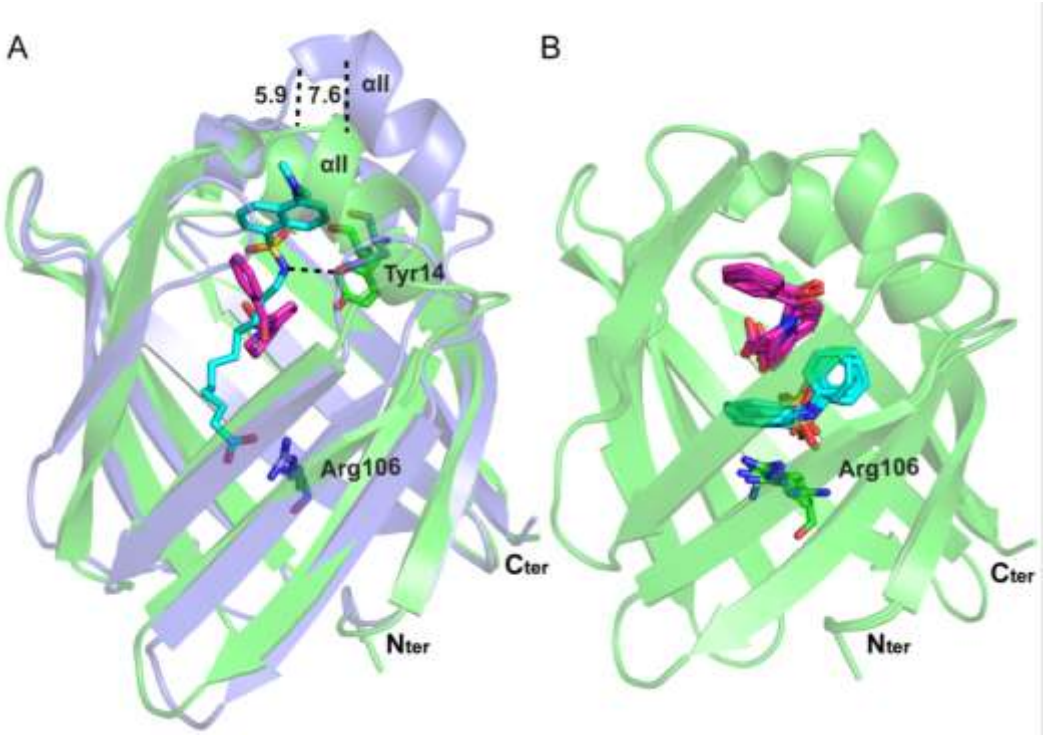

Figure 7. (A) Superimposition of the hIFABP–DAUDA complex (blue) with the hIFABP–ketorolac complex (green). Ketorolac (magenta) binding leads to a large change in the position of the αII helix. The distances measured between the C^{α} of Ile25 (7.6 Å) and Asn24 (5.9 Å) in the two structures are labeled. In the hIFABP DAUDA complex, Tyr14 (labeled) makes a polar contact with DAUDA (cyan). (B) Model of the ternary hIFABP–ANS–ketorolac complex showing the most highly ranked structures obtained following induced fit docking. ANS (cyan) binds towards the bottom of the hIFABP adjacent to Arg106. Ketorolac (magenta) binds further up the binding cavity and adopts a similar conformation in the NMR–derived model of the binary complex and in the docking model of the ternary complex.

Table 1: The observed ligand binding data for hIFABP measured by displacement of DAUDA compared with earlier reported values for rIFABP at 20 °C.

Ligands	**hIFABP Ki (μM)**	**rIFABP Ki (μM)***
ANS	31.1 ± 2.2	7.3 ± 0.2
DAUDA	0.3 ± 0.03	0.7 ± 0.02
Oleate	0.01 ± 0.004	N.D.
Fenofibric acid	6.1 ± 0.06	3.7 ± 0.1
Flufenamic acid	15.5 ± 0.4	10.9 ± 1.8
Tolfenamic acid	6.1 ± 0.1	7.2 ± 0.9
Clofibric acid	17.7 ± 0.02	110 ± 9.4
Flurbiprofen	23.2 ± 6.2	70 ± 11
Ibuprofen	263.5 ± 23	100 ± 8.8
Ketoprofen	82.4 ± 0.03	74 ± 3.4
Diclofenac	86.3 ± 0.05	520 ± 11
Ketorolac	9.4 ± 5.4	2300 ± 120

* Reported values by ANS displacement (11); N.D.: Not determined

Table 2: The thermodynamic parameters for ligand binding to hIFABP determined by ITC at 37 °C. Values are the mean of three independent measurements ± their standard deviations.

Ligands	**ΔH (**kcal mol^{-1}**)**	**TΔS (**kcal mol^{-1}**)**	**ΔG (**kcal mol^{-1}**)**	**N**	**K_D (μM)**	**% of ΔH in ΔG**
DAUDA	–11.5 ± 1.01	–2.38 ± 1.04	–9.14 ± 0.03	1.2 ± 0.1	0.36 ± 0.02	100
ANS	–3.66 ± 0.39	3.28 ± 0.52	–6.94 ± 0.15	0.9 ± 0.01	13.3 ± 3.04	53
Ketorolac	0.07 ± 0.01	6.09 ± 0.04	–6.02 ± 0.04	1.1 ± 0.1	56.7 ± 3.27	0
Fenofibric acid	–1.58 ± 0.62	6.04 ± 0.47	–7.62 ± 0.15	1.7 ± 0.06	4.41 ± 0.99	21
GW7647	–5.84 ± 0.84	2.55 ± 0.98	–8.39 ± 0.25	1 ± 0.2	1.3 ± 0.57	70
L165041	–10.2 ± 1.44	–2.92 ± 1.5	–7.31 ± 0.14	1 ± 0.1	7.2 ± 1.65	100
Fenofibrate	No binding observed					